Ninth International Conference on
THIN-WALLED STRUCTURES – ICTWS2023
Sydney, Australia, Nov 29 – Dec 1, 2023

CHANNEL SECTION LAMINATED BEAMS WITH NON-SYMMETRIES SUBJECTED TO FOUR-POINT BENDING

Filip Kazmierczyk*, Monika Zaczynska* and Tomasz Kubiak*

* Lodz University of Technology, Poland
e-mails: filip.kazmierczyk@p.lodz.pl, monika.zaczynska@p.lodz.pl, tomasz.kubiak@p.lodz.pl

Keywords: Lipped channel section beams; Laminates; Non-symmetric lay-ups; Buckling; Post-buckling; Lateral deflection.

Abstract. *Short beams with channel and lipped cross-section beams subjected to four-point bending have been investigated. The beams have been made of FRP-type laminate. The influence of non-symmetries in form of non-symmetric cross-section and non-symmetric layer arrangement on buckling and post-buckling behavior has been investigated. It was found that also for short beams under bending the distortion or lateral distortion buckling mode could exist. These types of buckling modes may lead to lateral deflection in the post-buckling range and finally decrease the load-carrying capacity. The non-symmetrical layer arrangement characterizes the non-obvious behavior due to different types of couplings. So, it was decided to analyze how the layer arrangements in beam with nonsymmetric cross-section impact on the lateral deflection, buckling load and/or load-carrying capacity. The finite element model validated by the results of experimental tests have been employed to perform parametric studies, i.e., checking the influence of non-symmetries on beam behavior. Performed investigations allowed to find relations between layer arrangements, cross-section, buckling and postbuckling behavior.*

1 INTRODUCTION

Thin-walled structures are widely used in engineering applications due to their lightweight, high strength, and high stiffness. When subjected to bending loads, thin-walled beams can undergo a complex behavior, including local and global buckling, and lateral-torsional buckling. In recent years, there has been extensive research in thin-walled beams under bending, and numerous studies have been conducted to investigate their behavior and optimize their design.

Nowadays, when mass optimization is a greater and greater issue, a wider materials range is used for manufacturing of construction parts. There exist multiple composite material types, and for load-carrying structures, it is possible to distinguish the following: Fiber Reinforced Polymer (CFRP, GFRP), Fiber Metal Laminate (FML), e.g., GLARE (GFRP with aluminum) [1, 2]. Due to their predictable behavior under operating load, the most popular laminate lay-ups are ones with typical layer arrangements (i.e., quasi-orthotropic, symmetric or antisymmetric cross-ply or angle-ply). Laminates with non-symmetrical lay-ups may lead to different behavior under load. In literature, they (the Hygro-Thermally Curvature Stable nonsymmetric laminates) were mainly analyzed as plates. York [3] considered laminates with non-standard lay-ups, e.g. (+60°, -60°, 0° and 90°). In his other paper together with Lee [4], they performed experimental validation of the proposed numerical CFRP laminate model with HTCS design, for samples matching Extension - Twisting coupling. More research concerning the use of non-symmetrical stacking sequences to design the structure behavior can be found exemplary in [5].

Many researchers focused to analyze such structures under bending. Pecce and Consenza [6] performed an analysis of FRP beams and columns to examine the local buckling phenomenon.

Sapkas and Kollar [7] investigated orthotropic I section beams under bending with non-symmetrical flanges. Lee et al. [8] performed a similar study; they also investigated mono-symmetrical I-beams with an emphasis on lateral buckling. One of the methods of laminate manufacturing is pultrusion; several scientists focused their research on that topic. Barbero and Raftoyiannis [9] studied pultruded I-beams under bending to investigate lateral and distortional buckling. Davalos et al. [10] examine the phenomenon of flexural-torsional buckling o I-beams. Nunes et al. [11] investigated experimentally and numerically I-beams under different bending conditions. Furthermore, they investigated the influence of hybrid pultruded composites, i.e., carbon fiber mixed with glass fiber, and the variation of their placement on the beam behavior. Autoclaving is a popular method of composite manufacturing, and many scientists analyzed such structures. Urbaniak et al. [12] investigated square GFRP beams subjected to pure bending. Using a similar test grip Kubiak et al. [13] performed experimental and numerical studies of channel section profiles subjected to bending in the flange plane.

A literature overview presented above, shows that it is hard to find papers devoted to the considered problem. Hence, it proves that the current knowledge of such beams' application is insufficient; therefore, additional research must be performed. Buckling starts in the compressed part of the beam. It is assumed to check the influence of smaller or even lack of the lip in the tensile part. Such approach can save the structure's weight without significantly decreasing stability and strength. Furthermore, there exists a possible application of non-standard, i.e., non-symmetrical layer arrangements to reduce lateral deflections. The study aims to analyze the influence of the stiffener (lip) width in the tensile part of the lipped channel section beam and different nonsymmetric layer arrangements under four-point bending. Parametric numerical analysis was performed for various layer arrangements with different couplings of the stiffness matrices. The numerical model was validated experimentally.

2 OBJECT OF THE STUDY

The lip channel section beams made of laminate with different layer arrangement and width of lip in compressed part have been tested. In Figure 1, the scheme of the considered cross-section with load is shown.

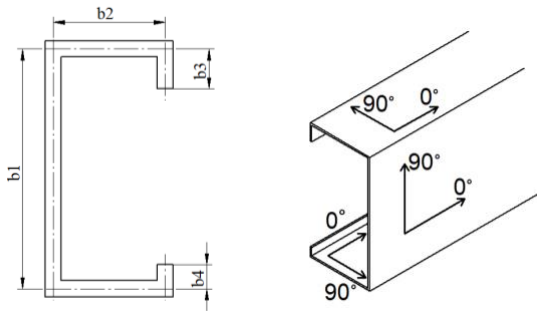

(a) (b)

Figure 1: Scheme of considered cross-section (a) and lay-up angles (b).

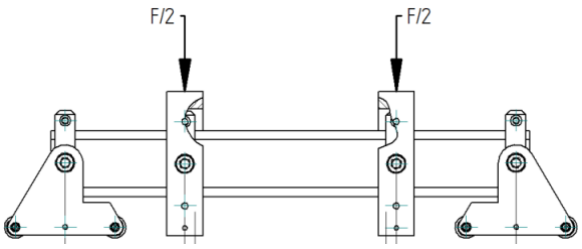

Figure 2: Scheme of beam support and load.

Dimensions of the web's width (b_1 = 80 mm), both flanges' width (b_2 = 40 mm) and widths of lip in the compressed part (b_3 = 10 mm) remaining constant, and the width of lip in the tensile part, which varies (b_4 = 0, 5, and 10 mm). Figure 1 presents also the scheme of angle lay-up on the walls of the beam. In the Figure 2 the scheme of the four-point bending test stand with load is shown.

The study was performed on beams made of E-glass 1200tex fibers immersed in NTPT THINPREG™ 402 epoxy resin. Mechanical properties were derived according to ASTM D3039 and ASTM D6641 standards. Table 1 lists the values of averaged mechanical properties of considered laminate.

Table 1: Averaged values of mechanical properties of the laminate

E_1 [GPa]	E_2 [GPa]	G_{12} [GPa]	ν_{12} [-]	T_1 [MPa]	T_2 [MPa]	C_1 [MPa]	C_2 [MPa]	S_{12} [MPa]
30	9.4	9.2	0.28	1260	43	620	140	130

Table 2: Layer arrangement of beams under consideration.

case ID	layer arrangement	laminate type	Considered θ [deg]
S1	45/-45/45/-45/-45/45/-45/45	$A_S B_0 D_F$	-
S2	0/90/0/90/90/0/90/0	$A_S B_0 D_S$	-
S3	45/-45/90/0/0/90/-45/45	$A_S B_0 D_F$	-
N1	45/45/45/45/-45/-45/-45/-45	$A_S B_t D_S$	-
N2	90/90/90/90/0/0/0/0	$A_S B_l D_S$	-
A1(θ) [14]	$\theta/(\theta\ -90)_2/\theta/-\theta/(90-\theta)_2/-\theta$	$A_S B_t D_S$	±22.5
N3(θ) [3]	90/0/θ/-θ/0/90/-θ/θ	$A_S B_S D_F$	±30, ±45, ±60
N3R(θ)	θ/-θ/90/0/-θ/θ/0/90	$A_S B_S D_F$	-30, -45, -60

In the present analysis, the influence of various laminate lay-ups on the beam behavior was studied. It was assumed that the laminates (walls of the beams) consist of 8 plies. Table 2 shows the considered layer arrangements with their annotation and matrices couplings. For following cases: A1, N3 and N3R, few angle of fiber arrangement were analyzed. Thus, 16 different layer arrangements were taken into consideration in numerical study. Each type of layer arrangement is denoted as follows, "S" for symmetrical lay-up, "N" for non-symmetrical and "A" for anti-symmetrical. Laminate stacking sequences were chosen based on the different couplings of the stiffness matrices. In the chosen layer arrangements, following load response coupling were achieved: A_S –simple laminate no in-plane coupling, A_F –shear-extension coupling, B_t- extension-twisting and shear-bending coupling, B_l- extension-bending coupling, B_S- extension-bending and shear-twisting coupling, D_S –simple laminate no out-of-plane coupling, D_F –twisting-bending coupling.

3 EXPERIMENTAL TESTS

Experimental tests were performed on the beam N3(30) with the layer arrangement [90/0/30/-30/0/90/-30/30]. Four specimens have been tested: two with symmetrical cross-section i.e., with equal width of lips in compressed and tensed part of the beam (b_3 = b_4 = 10 mm – see Fig. 1) and two specimens without the lip in tensed part of the beam (b_3 = 10 mm and b_4 = 0 mm).

The experiments have been performed using universal testing Instron® Machine and digital image correlation system Aramis®. The employed pieces of equipment allowed to collect following data: applied load, displacement of moving machine's cross head, and 3D deformation of examined samples. The scheme of experimental test stand is presented in Figure

3a. Figure 3 b presents the scheme of grips used to mount and load the specimens, depicting the points at which measure data were being collected.

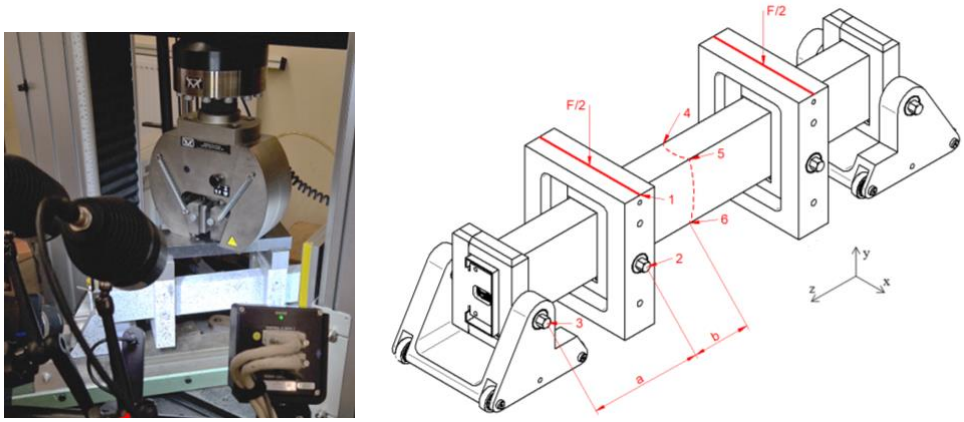

(a) (b)

Figure 3: Scheme of test stand (a) and grip with point of load and data collection (b).

The chosen points (Fig. 3b) and measured displacement allowed us to find the following parameters defining the beams' deflections and angles of rotation:

- w^* – the relative deflection of the web, calculated as relations between vertical displacements of web-lip join edge (point 4) and web-flange join edge (point 5): $u_{y4} - u_{y5}$.
- α_1 – the angle of rotation in the *yz* plane, based on the displacement of point 1 in *y*-direction: arctan (u_{y1}/a).
- α_2 – the angle of rotation in the *xz* plane, based on points 2 and 3 displacements in *z*-direction: arctan $[(u_{x2} - u_{x3})/a]$.
- α_3 – the angle of rotation in the *xz* plane, based on points 2, 5 and 6 displacements in *x*-direction: arctan $\{[(u_{x5} + u_{x6})/2 - u_{x2}]/b\}$.
- α_4 – the angle of rotation in the *xy* plane, based on points 5 and 6 displacements in *x*-direction: arctan $((u_{x5} - u_{x6})/b_1)$, b_1 see Fig. 1.

4 FEM MODEL

To perform parametric investigations the FEM commercial software (ANSYS APDL) was employed. Beams were modelled using four-node shell elements with six degrees of freedom at each node (SHELL181). The element size in the discrete model of the beam was assumed based on the authors' experience and checking this parameter's influence on results, and finally, the element edged length was assumed as approx. 1.5 mm. Eigenvalue analysis for buckling loads with corresponding modes determination as well as non-linear analysis to investigate the post-buckling behavior were performed. In the non-linear analysis the initial geometric imperfection with the magnitude of 0.1 of laminate wall thickness and the shape corresponding to the local buckling mode was assumed. The considered numerical model is shown in Figure 4. It corresponds to the four-point bending grip used to examine tested composite samples (c.f. Fig. 2). It consists of four pair of diaphragms which imitates real clamps, as in the test grip. In experimental tests, the boundary conditions and load are transferred by means of pivots. Therefore, in the numerical model, they are applied on lines lying in the mid of the web. Force was applied at nodes laying on two middle diaphragms, additional coupling was added to ensure constant vertical displacement (u_y = const.) of loading points. Vertical (*y*) and transverse (*x*) directions are set to zero at nodes lying on both ends of the model, while the longitudinal displacement (u_z) is set to zero at one node lying in the corner of one grip.

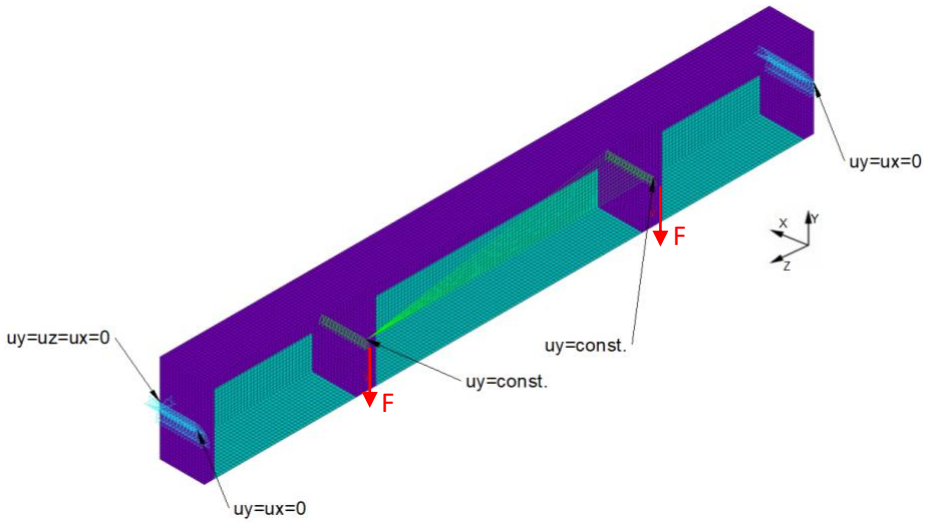

Figure 4: Discreet numerical model with applied four-point bending boundary conditions.

5 RESULTS

The results of experimental tests were used to validate the numerical model. The buckling load and ultimate bending moment were determined numerically and compared with the experimental results. In FE calculations, the buckling bending moment was obtained from the eigenvalue analysis. While in the laboratory test, the buckling load was obtained from equilibrium paths presented as a relation of load vs. angle of rotation α_3 and load vs. compressed flange deflection w^* (Fig. 5). They are derived according to method described in the paper of Paszkiewicz et. al [15] with accuracy up to around 10 Nm. It is possible to see, that the values of buckling load differ between both used methods (type of equilibrium path) in experimental results. The buckling loads M_{cr} determined based on relations between bending moment and flange deflection w^* are in the range 430 – 440 Nm for all tested beams, while in the case of equilibrium paths as relations between load and α_3 angle, the buckling loads M_{cr} were found in the range 480 – 490 Nm for beams with symmetrical cross-section and 420 – 440 Nm for beams with nonsymmetrical one. The buckling loads for beams with a symmetric cross-section obtained based on both considered types of equilibrium paths differ c.a. 10%. In such beams, the relative deflection w^* of the flange under compression decides the buckling, and the lateral deflections appear for the loads higher than the buckling one. However, in the case of beams with a nonsymmetrical cross-section, the lateral deflection in the pre-buckling range impacts increasing or changing the α_3 angle, which finally decides to buckle. Concluding, a buckling load determined based on the results of experimental tests for all tested beams is about 430 Nm.

It should be mentioned that the results from the numerical simulation taken to compare were obtained by performing linear buckling analysis (solving the eigenvalue problem). The above means that the buckling loads for real imperfect beams were compared with buckling loads for ideal theoretical structures. As it is well known, the initial geometrical imperfection and pre-buckling deflection significantly impact buckling. Also, it is worth pointing out that the buckling load determination based on experimental results is challenging [15]. Nevertheless, both numerically determined modes (flexural local buckling of beam's flange under compression - FLB, shear bending of beam's web - SB) with corresponding buckling loads are consistent with the estimated buckling load based on equilibrium paths. The buckling modes obtained numerically are presented in Figure 5.

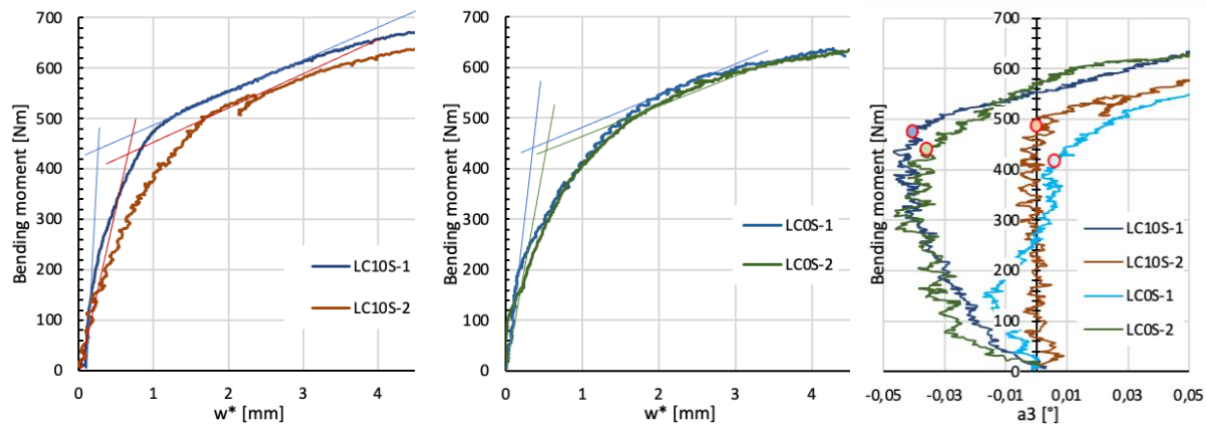

(a) (b) (c)

Figure 5: Buckling load determination based on equilibrium paths in form of bending moment vs. relative web deflection w^* for specimens with b_3 = 10 mm (a), b_3 = 0mm (b), and in form of bending moment vs. α_3 angle for all tested specimens (c).

Table 3: Comparison of critical buckling moment obtained from FEM and experiment.

ID	Critical bending moment M_{cr} [Nm]			Ultimate bending moment Mu [Nm]	
	Experiment		FEM	Experiment	FEM
	$M(\alpha_3)$	$M(w^*)$			
LC10-1	480	440	452^{SB}	680	612
LC10-2	490	430	466^{FLB}	679	
LC0-1	420	440	438^{SB}	637	669
LC0-2	440	430	466^{FLB}	635	

Comparing the differences between the values of buckling loads determined by FEM for beams with different cross-sections LC0 and LC10, it is seen that the buckling load corresponding to flexural buckling modes are the same. Still, comparing buckling corresponding to shear mode, the buckling loads differ and depend on the cross-section type - lower is for the beam with nonsymmetric cross-section LC0 for shear buckling mode. Summing up the above and considering the deflections corresponding to buckling modes presented in Figures 5 and 6, it can be said that the buckling mode of real beams (Fig. 7) is a kind of sum of those two determined in linear buckling analysis (FEM).

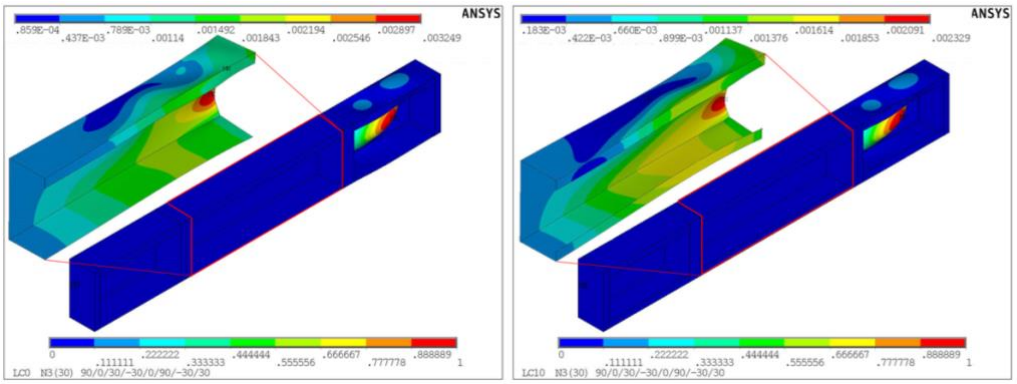

(a) (b)

Figure 5: Shear buckling mode with depicted deflection in the middle part of the beam for the case of the cross-section LC0 (a) and LC10 (b).

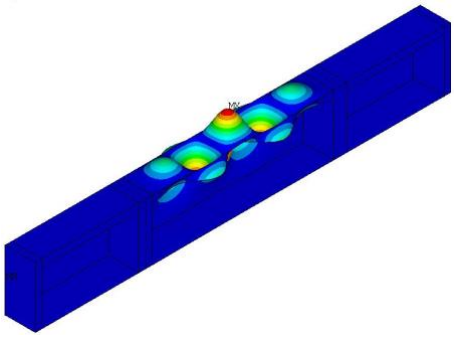

Figure 6: Flexural local buckling mode.

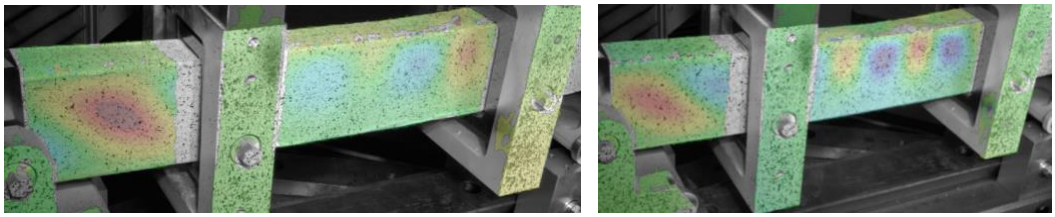

(a) (b)

Figure 7: Buckling mode of tested specimens for beam with layer arrangement N3(30) and two different cross-sections: LC0 (a), LC10 (b).

Table 3 presents also the comparison of the ultimate bending moments M_u. While for the beam LC10, experimental results are slightly higher than numerical predictions, for LC0 beams, the opposite tendency is obtained. Nevertheless, the results' difference is up to 10% which is an acceptable error and confirms the correctness of the adopted FE model and its further application in the parametric study.

Parametric analysis was performed for all sixteen considered layers' arrangements (Table 2) for three widths of stiffener b_4 = 0; 5; and 10 mm.

Table 4 presents values of critical buckling moment (the lowest – 1st, and corresponding to flexural local buckling mode), ultimate bending moment as well as the ratio ultimate bending moment to critical one obtained in numerical simulations. In the case when in Table 4, the values of the lowest buckling load (1st) and buckling load corresponding to flexural local buckling mode (FLB) are the same (only one value is presented) this means the lowest buckling load corresponds to flexural local buckling mode (FLB). In the other cases (except for those highlighted in yellow in Table 4), the lowest buckling load correspond to the shear buckling mode (see Fig. 5). Mentioned above cases, which are highlighted in yellow, corresponding to the buckling mode presented in Figure 8, and then the buckling loads corresponding to both buckling modes (shear buckling and flexural local buckling) are very close.

Furthermore, Table 4 shows the percentage difference of buckling loads for beams with horizontally symmetric cross-sections (LC10) and unsymmetric ones (LC0). It was calculated according to the following formula:

$$\%\ difference = \frac{V_{LC0} - V_{LC10}}{V_{LC10}} * 100\% \tag{1}$$

where V_{LC10} and V_{LC0} denote compared values for both cases of beams' cross-sections.

The positive value obtained from Eq. (1) means that compared moment for the case LC0 is higher than for LC10, while for the negative result, the case LC0 is less. In all columns of Table 4, the maximum

and minimum values for presented results have been enlightened with different colors - the red one depicts the maximum value and the blue one the minimum.

Table 4: Buckling and ultimate moment as well as their ratio for all considered laminate cases.

ID of layup	Cross-section type									M_{cr}^{1st}	M_u
	LC10			LC5			LC0				
	M_{cr}^{1st} / M_{cr}^{FLB} [Nm]	M_u [Nm]	M_u / M_{cr}^{1st} [-]	M_{cr}^{1st} / M_{cr}^{FLB} [Nm]	M_u [Nm]	M_u / M_{cr}^{1st} [-]	M_{cr}^{1st} / M_{cr}^{FLB} [Nm]	M_u [Nm]	M_u / M_{cr}^{1st} [-]	LC10 to LC0 difference [%]	LC10 to LC0 difference [%]
S1	422 454	566	1.34	417 457	568	1.36	409 455	542	1.33	-3.1	-4.2
S2	458 467	552	1.21	452 470	580	1.28	444 468	602	1.36	-3.1	9.1
S3	442 459	568	1.29	436 462	583	1.34	427 460	627	1.47	-3.4	10.4
A1(+22.5)	467	571	1.22	466 469	571	1.23	458 467	627	1.37	-1.9	9.8
A1(-22.5)	467	569	1.22	466 469	582	1.25	458 467	597	1.30	-1.9	4.9
N1	368	497	1.35	371	495	1.33	369	490	1.33	0.3	-1.4
N2	408	510	1.25	404 410	521	1.29	396 407	542	1.37	-2.9	6.3
N3(+30)	452 466	612	1.35	446 468	630	1.41	441 466	669	1.52	-2.4	9.3
N3(-30)	452 466	604	1.34	446 468	620	1.39	441 466	669	1.52	-2.4	10.8
N3(+45)	462 463	570	1.23	455 465	594	1.31	446 463	635	1.42	-3.5	11.4
N3(-45)	462 463	558	1.21	455 465	577	1.27	446 463	565	1.27	-3.5	1.3
N3(+60)	458	518	1.13	461	544	1.18	455 458	565	1.24	-0.7	9.1
N3(-60)	458	513	1.12	461	630	1.37	455 458	568	1.25	-0.7	10.7
N3R(-30)	453 469	608	1.34	447 471	619	1.38	439 469	647	1.47	-3.1	6.4
N3R(-45)	462 464	560	1.21	455 465	586	1.29	446 464	614	1.38	-3.5	9.6
N3R(-60)	456	510	1.12	459	593	1.29	454 456	561	1.24	-0.4	10.0

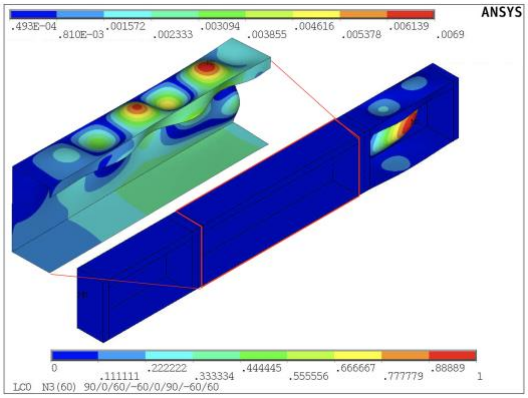

Figure 8: Shear buckling mode for beam LC0, and lay-ups N3(±60) and N3R(-60).

To analyze the influence of the couplings in laminates due to their layer arrangement on beams behavior, the values of dimensionless coefficients of stiffness reduction α_x, α_y, α_{xy} (Eqs. 2) were analyzed as it is proposed by Teter et. al. [16]. The closer to the unity of these stiffness reduction coefficients the lower impact of the coupling stiffness matrix B.

$$\alpha_x = 1 - \frac{B_{11}^2}{D_{11}A_{11}}, \qquad \alpha_y = 1 - \frac{B_{22}^2}{D_{22}A_{22}}, \quad \alpha_{xy} = 1 - \frac{B_{66}^2}{D_{66}A_{66}}, \tag{2}$$

These coefficients with the nondimensional elements of laminate stiffness matrix A_{11*} and D_{11*} ($A_{11*} = A_{11}/A_{11max}$ and $D_{11*} = D_{11}/D_{11max}$ i.e., A_{11} or D_{11} for given layer arrangement divided by the highest positive value from all analyzed cases) and information about stiffnesses D16 and D26 showing shear bending couplings are presented in Table 5.

Table 5. Laminate stiffness matrix elements analyze.

case ID	α_x	α_y	α_{xy}	A_{11*}	D_{11*}	D_{16} and D_{26}
S1	1	1	1	0.66	0.56	$D_{16} = D_{26} \neq 0$
S2	1	1	1	0.96	1.00	$D_{16} = D_{26} = 0$
S3	1	1	1	0.81	0.54	$D_{16} = D_{26} \neq 0$
A1(±22.5)	1	1	1	0.81	0.75	$D_{16} = D_{26} = 0$
N1	1	1	1	0.66	0.56	$D_{16} = D_{26} = 0$
N2	0.6998	0.6998	1	0.96	0.81	$D_{16} = D_{26} = 0$
N3(±30)	0.9997	0.9768	0.9600	1.00	0.75	$D_{16} \neq D_{26}$
N3(±45)	0.9925	0.9944	0.9466	0.81	0.59	$D_{16} = D_{26} \neq 0$
N3(±60)	0.9677	0.9997	0.9600	0.70	0.49	$D_{16} \neq D_{26}$
N3R(-30)	0.9997	0.9768	0.9600	1.00	0.75	$D_{16} \neq D_{26}$
N3R(-45)	0.9925	0.9944	0.9466	0.81	0.59	$D_{16} = D_{26} \neq 0$
N3R(-60)	0.9677	0.9997	0.9600	0.70	0.49	$D_{16} \neq D_{26}$

Let's analyze, how the buckling M_{cr} and ultimate M_u moments change with the change of the cross-section. Comparing the change between beams with cross-sections LC10 and LC0, buckling moments decrease (only in one case a slight increase appears - N1). The situation is different in the case of load-carrying capacity, that comparison 14 from 16 analyzed layer arrangements increases the ultimate moment M_u. Additionally, it can be said, that 5 of all considered cases lead to an increase in the load-carrying capacity of more than 10%. The highest buckling load was obtained for beam LC10 with lay-up A1(±22.5), while the highest load-carrying capacity was for LC0 N3(±30). Analyzing the influence of layer arrangements shows that lay-up A1 is one of the two cases where the

extension-twisting and shear-bending coupling B_t exist (non-zero B_{16} and B_{26}). Nevertheless, the second is the case denoted as N1 for which the beam under investigation has the lowest buckling load, which means that the non-only type of couplings but also stiffnesses decide the value of the buckling load (e.g., stiffness matrix element D_{11} for A1 lay-up is c.a. 25% higher than for N1). The highest load-carrying capacity was obtained for the case of layer arrangement with coupling type B_SD_F (see Table 2), where B_S denotes extension-bending and shear-twisting coupling, and D_F - twisting-bending coupling.

The case N3(±30) within all considered with the same type of coupling has less than one all stiffness reduction coefficients and the lowest stiffness reduction coefficient α_y (see Table 5). Comparing all cases of layer arrangement, it can be said, that this type of coupling (B_SD_F) can positively be impacting the increase of load-carrying capacity for open-section cross-section beams under bending.

Table 6. Ultimate rotation angles for LC10 and LC0 cross sections for all considered laminate lay-ups.

case ID	α_{1u}	α_{2u} [°]	α_{3u}	α_{1u}	α_{2u} [°]	α_{3u}
	Cross-section type					
	LC10			LC0		
S1	1.44	0.105	0.505	1.42	0.351	0.506
S2	1.47	0.123	0.742	1.88	0.378	0.242
S3	1.47	0.120	0.683	2.02	0.635	0.859
A1(+22.5)	1.51	0.124	0.772	1.99	0.589	0.855
A1(-22.5)	1.54	0.154	0.964	1.92	0.563	0.718
N1	1.33	0.058	0.441	1.37	0.322	0.514
N2	1.47	0.187	0.814	1.79	0.297	0.279
N3(+30)	1.51	0.117	0.613	1.88	0.212	0.047
N3(-30)	1.51	0.104	0.61	1.88	0.212	0.047
N3(+45)	1.47	0.107	0.691	2.15	0.65	0.836
N3(-45)	1.51	0.156	0.971	2.38	0.602	0.389
N3(+60)	1.51	0.099	0.717	2.43	0.644	0.399
N3(-60)	1.56	0.14	0.935	2.47	0.562	0.054
N3R(-30)	1.56	0.171	0.98	1.833	0.291	0.154
N3R(-45)	1.51	0.149	0.922	2.24	0.632	0.568
N3R(-60)	1.51	0.09	0.754	2.43	0.666	0.465

Table 6 presents the ultimate vertical and both horizontal rotation angles for two opposite cross-section types. Horizontally symmetrical one (LC10) and the most non-symmetrical one (LC0). First, it is worth mentioning that the values of the vertical angles are small and extremely small for horizontal ones. For LC10 the highest value of vertical rotation angle is obtained for lay-ups N3(-60) and N3R(-30), while for LC0 cross-section beam for N3(-60). The lowest α_{1u} angle was obtained for the N1 layer arrangement in both cases of the beam's cross-section LC10 and LC0 - which also corresponds to the lowest buckling and ultimate loads.

Concerning horizontal rotation angles α_{2u} and α_{3u}, it is visible that different layer arrangements indicate the highest or lowest values of rotation angles, which are not corresponding with the extremal values of load-carrying capacity. From a practical point of view, the interesting is the case with the lowest angle of transverse rotation and the highest load-carrying capacity but challenging to find. For example, for LC10 samples, the highest value of α_{2u} angle is represented by a beam with layer arrangement N2, and this angle is 60%

higher than for the sample with N3(30) lay-up characterized by the highest ultimate load. The lowest α_{2u} angle of rotation was obtained for the beam with N1 laminate type, but it is a case with the lowest load-carrying capacity.

The angle α_{3u} was also considered to analyze the transverse behavior of the beams. The highest value of α_{3u} angle was obtained for beam LC10 with N3R(-30) laminate type and in the case of beam's cross-section LC0 for lay-up S3.

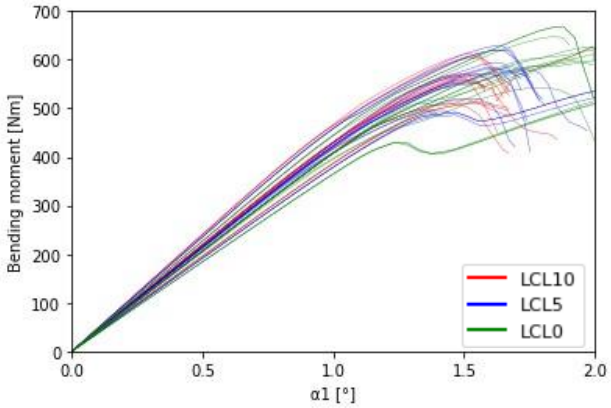

Figure 9: Vertical behavior of LC10-5-0 beams for all layer arrangements.

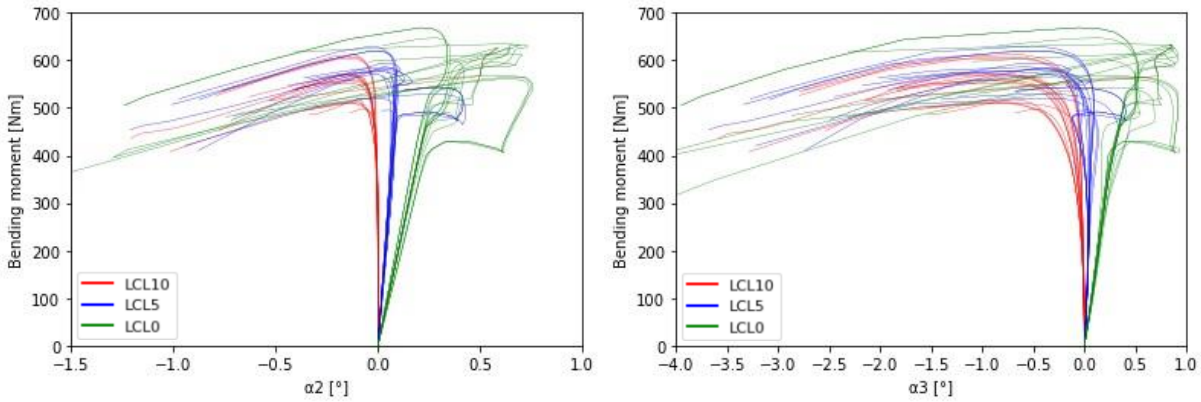

(a) (b)

Figure 10: Horizontal (a, b) behavior of LC10-5-0 beams for all layer arrangements.

In Figures 9 and 10 graphs of the vertical (α1) and both horizontal (α2, α3) rotation angles are shown for all considered lay-ups and three cross-sections, to visualize the general behavior of a particular cross-section. In Figure 10 the lowest horizontal deflections are observed for LC5 samples. The beams with the cross-section LC10 deflect to negative values and LC0 to positive ones, while LC5 are around zero, so the most desirable behavior. It is observed as well for α2 and α3 rotation angles.

6 CONCLUSIONS

Analysis of lipped channel section beams with non-symmetrical lip distribution and various layer arrangements was performed. The finite Element Method was used to analyze the problem based on the results of experimental outcomes. Experimental tests were performed in the test grip, which should allow the beam to rotate more freely between the support and the place of force appliance in the flange plane. Real four-point bending was employed. Beams with one layer arrangement were chosen based on previous research [13] (i.e., N3(30) lay-up), for which three different cross-sections with alternating tensile part lip widths were manufactured and

examined. A deep numerical investigation was performed by analyzing sixteen different layer arrangements chosen based on different laminate stiffness matrixes coupling (see Table 2). The parametrical numerical study aimed to find a non-standard lay-up for which the lowest horizontal deflection will appear. First, it is necessary to mention that the lowest lateral deflections were found for the for LC5 cross-section regardless of the layer arrangement. However, due to the possibility of behavior design; it was found that it is possible to find a non-symmetrical lay-up for a horizontally non-symmetrical cross-section which will provide the lowest lateral deformations, as well as ones with the highest buckling load and load-carrying capacity.

REFERENCES

[1] Vogelesang L.B., Vlot A., "*Development of fibre metal laminates for advanced aerospace structures", J. Mater. Process. Technol.*, **103**, 1-5, 2000.

[2] Wu G., Yang J.-M., "*The mechanical behavior of GLARE laminates for aircraft structures*", *JOM* **57**, 72-79, 2005.

[3] York, C., "*Tapered hygro-thermally curvature-stable laminates with non-standard ply orientations*", *Composites Part A Appl. Sci. Manuf.*, **44**, 140-148, 2013.

[4] York C.B., Lee K.K., "*Test validation of extension-twisting coupled laminates with matched orthotropic stiffness*", *Composite Structures*, **242**, 112142, 2020.

[5] Sasikumar A., García-Rodríguez S., Arbeláez J., Trias D., Costa J., "*On how unsymmetrical laminate designs with tailored ply clusters affect compression after impact strength compared to symmetric baseline", Composite Structures*, **238**, 111958, 2020.

[6] Pecce M., Cosenza E., "*Local buckling curves for the design of FRP profiles", Thin-Walled Structures*, 37, 207-222, 2000.

[7] Sapkas A., Kollar L. P., "*Lateral-torsional buckling of composite beams*". *International Journal of Solid and Structures*, 39, 2939-2963, 2002.

[8] Lee J., "*Lateral buckling analysis of thin-walled laminated composite beams with monosymmetric sections", Engineering Structures*, **28**, 1997-2009, 2006.

[9] Barbero E. J., Raftoyiannis I. G., "*Lateral and distortional buckling of pultruded I-beams", Composite Structures*, 27, 261-268, 1994.

[10] Davalos J. F., Qiao P., Salim H. A., "*Flexural-torsional buckling of pultruded fiber reinforced plastic composite I-beams experimental and analytical evaluations", Composite Structures*, **38**, 241-250, 1997.

[11] Nunes F., Correia J. R., Silvestre N., "*Structural behavior of hybrid FRP pultruded beams Experimental, numerical and analytical studies", Thin-Walled Structures*, **106**, 201-217, 2016.

[12] Urbaniak M., Swiniarski J. Czapski P., Kubiak T., "*Experimental investigations of thin-walled GFRP beams subjected to pure bending", Thin-Walled Structures*, **107**, 397-404, 2016.

[13] Kubiak T., Urbaniak M., Kazmierczyk F., "*The Influence of the Layer Arrangement on the Distortional Post-Buckling Behavior of Open Section Beams", Materials*, **13**, 3002, 2020.

[14] Winckler, S.J., "*Hygrothermally curvature stable laminates with tension-torsion coupling", J. Am. Helicopter Soc*., **31**,56-58, 1985.

[15] Paszkiewicz M., Kubiak T., "*Selected problems concerning determination of the buckling load of channel section beams and columns", Thin-Walled Struc*tures, **93**, 112-121, 2015.

[16] Teter A., Kolakowski Z., Mania R. J., "*Effect of selected elements of the coupling stiffness submatrix on the load-carrying capacity of hybrid columns under compression*", *Composite Structures*, **180**, 140-147, 2017.